

Lower bound on the proton charge radius from electron scattering data

Franziska Hagelstein

Albert Einstein Center for Fundamental Physics, Institute for Theoretical Physics, University of Bern, Sidlerstrasse 5, CH-3012 Bern, Switzerland

Vladimir Pascalutsa

Institut für Kernphysik and Cluster of Excellence PRISMA, Johannes Gutenberg Universität Mainz, D-55128 Mainz, Germany

Abstract

The proton charge-radius determinations from the electromagnetic form-factor measurements in electron-proton scattering require an extrapolation to zero momentum transfer ($Q^2 = 0$) which is prone to model-dependent assumptions. We show that the data at finite momentum transfer can be used to establish a rigorous lower bound on the proton charge radius. Using the available ep data at low Q^2 , we obtain $R_E > 0.850(1)$ fm as the lower bound on the proton radius. This reaffirms the discrepancy between the ep and muonic-hydrogen values, while bypassing the model-dependent assumptions that go into the fitting and extrapolation of the ep data.

Keywords: Charge radius, proton size, form factors, charge distribution, electron scattering

Contents

1	Introduction	1
2	Basic ingredients of the radius extraction	2
3	Positivity bounds	2
4	Results from ep scattering data	4
4.1	Direct determination	4
4.2	Overall normalization factor	5
4.3	Towards a normalization-free bound	5
5	Conclusion	6
	Acknowledgements	7
	References	7

1. Introduction

The proton charge radius is traditionally accessed in elastic electron-proton (ep) scattering at small momentum transfers (low Q) [1, 2]. Recently, however, the accuracy of this method has been questioned in the context of the *proton-radius puzzle*, which is partially attributed to the discrepancy between the 2010 ep scattering value of Bernauer et al. [3, 4] and the muonic-hydrogen (μH) extraction of the proton radius [5, 6], see Fig. 1. Meanwhile, as seen from the figure, the different extractions based on ep -scattering data have covered a whole range of values and hardly add-up into a coherent picture.

A “weak link” of the proton-radius extractions from ep experiments is the extrapolation to zero momentum transfer. Namely, while the data taken in some finite- Q^2 range can directly be mapped into the proton (electric and magnetic) Sachs form factors $G_E(Q^2)$ and $G_M(Q^2)$, the radii extractions require the derivatives of those at $Q^2 = 0$, e.g.: $R_E = \sqrt{-6 G'_E(0)}$. As much as one believes that the slope at 0 is largely determined by the behavior at finite Q^2 , it is not easy to quantify this relation with the necessary precision. The issues of fitting and extrapolation of the form-factor data have lately been under intense discussion, see, e.g., Refs. [14, 21–23]. Similar extrapolation problems should exist in the extractions based on lattice QCD, since the lowest momentum-transfer therein is severely limited by the finite volume.

Here, we show that the form-factor data at finite Q^2 provide a *lower bound* on the proton charge radius. A determination of this bound needs no extrapolation, therefore no major model assumptions, and should be based solely on experimental (or lattice) data. At the same time, given that some of the conventional extractions from ep data show a considerably larger radius than the μH value, a strict lower bound, based purely on data, is potentially useful in understanding this discrepancy.

In what follows, we briefly recall the basic formulae in Sec. 2, introduce the quantity proposed to serve as the charge-radius bound in Sec. 3, obtain an empirical value for it based on proton electric form-factor data in Sec. 4 and conclude in Sec. 5.

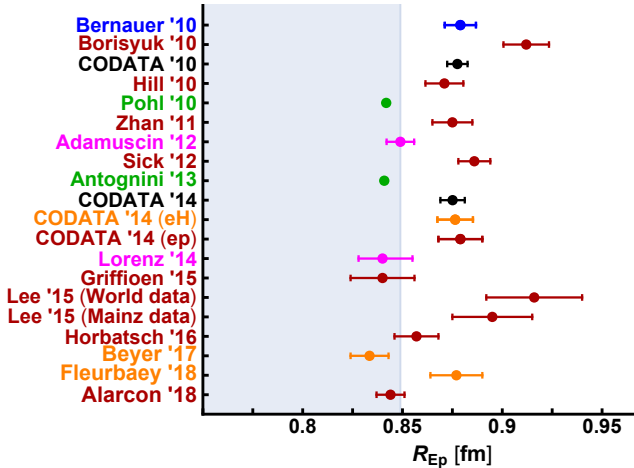


Figure 1: Summary of different proton charge-radius extractions. A) CODATA recommended charge radii in black: '10 [7], '14 [8]. B) hydrogen and deuterium spectroscopy in orange: Beyer '17 [9], Fleurbäy '18 [10]; C) muonic-hydrogen spectroscopy in green: Pohl '10 [5], Antognini '13 [6]; D) electron-proton scattering experiments in red: Borisyuk '10 [11], Hill '10 [12] (z expansion), Zhan '11 [13] (recoil polarimetry), Sick '12 [14], Griffioen '15 [15], Lee '15 [16], Horbatsch '16 [17] (fit with chiral perturbation theory input for higher moments); E) electron-proton scattering fits within a dispersive framework in magenta: Adamuscin '12 [18], Lorenz '14 [19], Alarcon '18 [20]; F) electron-proton scattering data from Bernauer '10 [3] in blue. G) the values excluded by lower bound from this work are indicated by the light-blue band.

2. Basic ingredients of the radius extraction

Let us recall that a spin-1/2 particle, such as the proton, has two electromagnetic form factors. These are either the Dirac and Pauli form factors: $F_1(Q^2)$ and $F_2(Q^2)$; or, the electric and magnetic Sachs form factors:

$$G_E(Q^2) = F_1(Q^2) - \frac{Q^2}{4M^2} F_2(Q^2), \quad (1a)$$

$$G_M(Q^2) = F_1(Q^2) + F_2(Q^2), \quad (1b)$$

with M the particle mass. The Sachs form factors can be interpreted as the Fourier transforms of the charge and magnetization distributions, $\rho_E(\vec{r})$ and $\rho_M(\vec{r})$, in the Breit frame. Strictly speaking, this relation holds only for spherically symmetric densities, in which case one has, see e.g. Ref. [24]:

$$G_E(Q^2) = 4\pi \int_0^\infty dr r^2 j_0(Qr) \rho_E(r), \quad (2a)$$

$$\frac{G_M(Q^2)}{1 + \kappa} = 4\pi \int_0^\infty dr r^2 j_0(Qr) \rho_M(r), \quad (2b)$$

where $j_0(x) = \frac{\sin x}{x}$ is the spherical Bessel function, and κ is the anomalous magnetic moment of the proton. Note that these are Lorenz-invariant expressions, hence, the spherically symmetric charge and magnetization distributions are, just as the form factors, Lorenz-invariant quantities.

The radii are introduced through the density moments, which, for even k , can be given by the form-factor derivatives at 0:

$$\begin{aligned} \langle r^k \rangle_E &\equiv 4\pi \int_0^\infty dr r^2 r^k \rho_E(r) \\ &\stackrel{\text{even } k}{=} (-1)^{k/2} \frac{(k+1)!}{(k/2)!} G_E^{(k/2)}(0); \end{aligned} \quad (3)$$

and similarly for the magnetic radii with ρ_E replaced by ρ_M , and G_E replaced by $G_M/(1 + \kappa)$, respectively. Therefore, the Taylor expansion of the form factor around $Q^2 = 0$ is written as:

$$\begin{aligned} G_E(Q^2) &= \sum_{n=0}^{\infty} \frac{(-1)^n}{(2n+1)!} \langle r^{2n} \rangle_E Q^{2n} \\ &= 1 - \frac{1}{6} \langle r^2 \rangle_E Q^2 + \frac{1}{120} \langle r^4 \rangle_E Q^4 + \dots \end{aligned} \quad (4)$$

The subject of interest is the root-mean-square (rms) radius (or, simply the charge radius): $R_E = \sqrt{\langle r^2 \rangle_E}$. Ideally, it could be extracted by fitting the first few terms of the above Taylor expansion of the form factor to the experimental data at low Q^2 . In practice, however, this does not work. The main reason is that the convergence radius of the Taylor expansion is limited by the onset of the pion-production branch cut for time-like photon momenta at $Q^2 = -4m_\pi^2$ (the nearest singularity, as far as the strong interaction is concerned), and there are simply not many ep data for $Q^2 \ll 4m_\pi^2 \approx 0.08 \text{ GeV}^2$.

A viable approach to fit to higher Q^2 is, instead of the Taylor expansion, to use a form which takes the singularities into account. This is done in the z -expansion [12] and dispersive fits [18–20]. These approaches have, however, other severe limitations. The z -expansion only deals with the first singularity and therefore extends the convergence radius to $3m_\pi^2$ only. The dispersive approach is based on an exact dispersion relation for the form factor:

$$G_E(Q^2) = 1 - \frac{Q^2}{\pi} \int_{4m_\pi^2}^{\infty} dt \frac{\text{Im } G_E(t)}{t(t+Q^2)}, \quad (5)$$

which, in principle, accounts for all singularities. Unfortunately, it requires the knowledge of the spectral function, $\text{Im } G_E(t)$, which is not directly accessible in experiment, and needs to be modeled. Chiral perturbation theory can only provide a description of this function in the range of $t \ll 1 \text{ GeV}$. Despite the recent progress in the empirical description of the spectral function [25], the problem of model dependence of the radius extraction in the dispersive approach remains to be non-trivial.

3. Positivity bounds

Given the aforementioned issues in extracting the charge radius from form-factor data, we turn to establishing a bound on the radius, rather than the radius itself. The

advantage is that the bound will follow from the finite- Q^2 data alone and needs no extrapolations or model assumptions.

To this end we consider the following quantity:

$$R_E^2(Q^2) \equiv -\frac{6}{Q^2} \ln G_E(Q^2), \quad (6)$$

which in the real-photon limit yields the radius squared:

$$\lim_{Q^2 \rightarrow 0} R_E^2(Q^2) = -6 \frac{G'_E(Q^2)}{G_E(Q^2)} \Big|_{Q^2=0} = R_E^2. \quad (7)$$

As will be argued in Sec. 3, the spacelike ($Q^2 \geq 0$) proton form factor is bounded from above:

$$G_E(Q^2) \leq 1, \quad (8)$$

and hence, the above log-function is positive, $R_E^2(Q^2) \geq 0$. Furthermore, if G_E falls with increasing Q^2 not faster than by a power law, then $R_E^2(Q^2)$ falls as well. The analytic properties of G_E , in the absence of zeros, are inherited by its logarithm. The subtracted dispersion relation (5) for the form factor then leads to an unsubtracted one for R_E^2 :

$$R_E^2(Q^2) = \frac{1}{\pi} \int_{4m_\pi^2}^{\infty} dt \frac{\text{Im} R_E^2(t)}{t + Q^2}, \quad (9)$$

where $\text{Im} R_E^2(t) = (6/t)\varphi_E(t)$, and $\varphi_E(t) \geq 0$ is the phase defined through $G_E(t) = |G_E(t)|e^{i\varphi_E(t)}$. This dispersion relation shows that the function is monotonic in the spacelike region. The latter allows one to establish a *lower bound on the radius*:

$$R_E^2(Q^2) \leq R_E^2, \quad \text{for } Q^2 \geq 0. \quad (10)$$

Substituting in here the Taylor expansion Eq. (4), one has (up to $\mathcal{O}(Q^4)$):

$$R_E^2(Q^2) = R_E^2 - \left(\frac{1}{20} \langle r^4 \rangle_E - \frac{1}{12} R_E^4\right) Q^2, \quad (11)$$

and so, in order for the bound to hold at arbitrarily low Q^2 , the forth and second moments must satisfy the following inequality:¹

$$\sqrt{\frac{3}{5} \langle r^4 \rangle_E} > R_E^2. \quad (12)$$

We have checked that this non-trivial hierarchical condition on the radii, which follows from the lower bound Eq. (10), is verified in existing empirical parametrizations of the proton form factor, of which the dipole form, $G_E(Q^2) = [1 + Q^2/(0.71 \text{ GeV}^2)]^{-2}$, is the simplest one.

¹Based on Eq. (9), one can claim that $R_E^2(Q^2)$ is completely monotonic, i.e.: $(-1)^n d^n R_E^2(Q^2)/d(Q^2)^n \geq 0$, from which the lower bounds on other radii can be derived. The lowest values of the radii are given in terms of the charge radius R_E , and can all be obtained from Taylor-expanding the following form of the form factor: $G_E^{(\text{min})}(Q^2) = \exp(-\frac{1}{6} R_E^2 Q^2)$.

The fact that $R_E^2(Q^2)$ is monotonically increasing towards $Q^2 = 0$, means that the best bound is obtained at lowest accessible Q^2 . In practice, however, it depends on the size of the experimental errors, including the uncertainty in the overall normalization of the form factor. We discuss this in detail in Sec. 4, when obtaining the empirical value of the bound from experimental data. In the rest of this section we focus on the proof of Eq. (8).

The unitary bound on the proton form factor, given in Eq. (8), and subsequently the radius bound, given in Eq. (10), follow from *positivity* of the corresponding charge density distribution: $\rho_E(r) \geq 0$. Indeed, from Eq. (2a),

$$G_E(0) - G_E(Q^2) = 4\pi \int_0^\infty dr r^2 [1 - j_0(Qr)] \rho_E(r), \quad (13)$$

with the property of the Bessel function $j_0(x) \leq 1$, and the positivity of $\rho_E(r)$, we can see that the integrand on the right-hand side is positive definite, and Eq. (8) follows upon substituting $G_E(0) = 1$ on the left-hand side.

There is a concern [27] that the proton charge density is not necessarily positive definite, and only the transverse charge density is ($\rho_\perp(b) \geq 0$). The latter relates to the Dirac form factor through the two-dimensional Fourier transform:

$$F_1(Q^2) = 2\pi \int_0^\infty db b J_0(Qb) \rho_\perp(b), \quad (14)$$

where $J_0(x)$ is the cylindrical Bessel function. However, the positivity of the transverse charge density is sufficient to prove the unity bound of Eq. (8). To see this, one may apply the previous argument [cf. Eq. (13)] to Eq. (14) using $J_0(x) \leq 1$, and derive the bound on the Dirac form factor:

$$F_1(Q^2) \leq 1. \quad (15)$$

Then, the unitary bound on G_E follows from its definition in terms of the Dirac and Pauli form factors, see Eq. (1a), by taking into account the conditions $F_1(Q^2) \leq 1$ and $F_2(Q^2) \geq 0$. The latter is valid for the proton in at least the low- Q region, as can be seen empirically from $F_2(0) = \kappa$, with $\kappa \simeq 1.79$ the anomalous magnetic moment of the proton.

While the unity bound on G_E follows from the positivity of $\rho_E(r)$, the reverse is not necessarily true. Therefore, the proof based on the positivity of the transverse charge density $\rho_\perp(b)$ does not necessarily imply the positivity of $\rho_E(r)$. Introducing $\rho_1(r)$ as the three-dimensional Fourier-transform of the Dirac form factor, we have

$$F_1(Q^2) = 4\pi \int_0^\infty dr r^2 j_0(Qr) \rho_1(r), \quad (16)$$

and matching it to Eq. (14), we obtain its relation to the

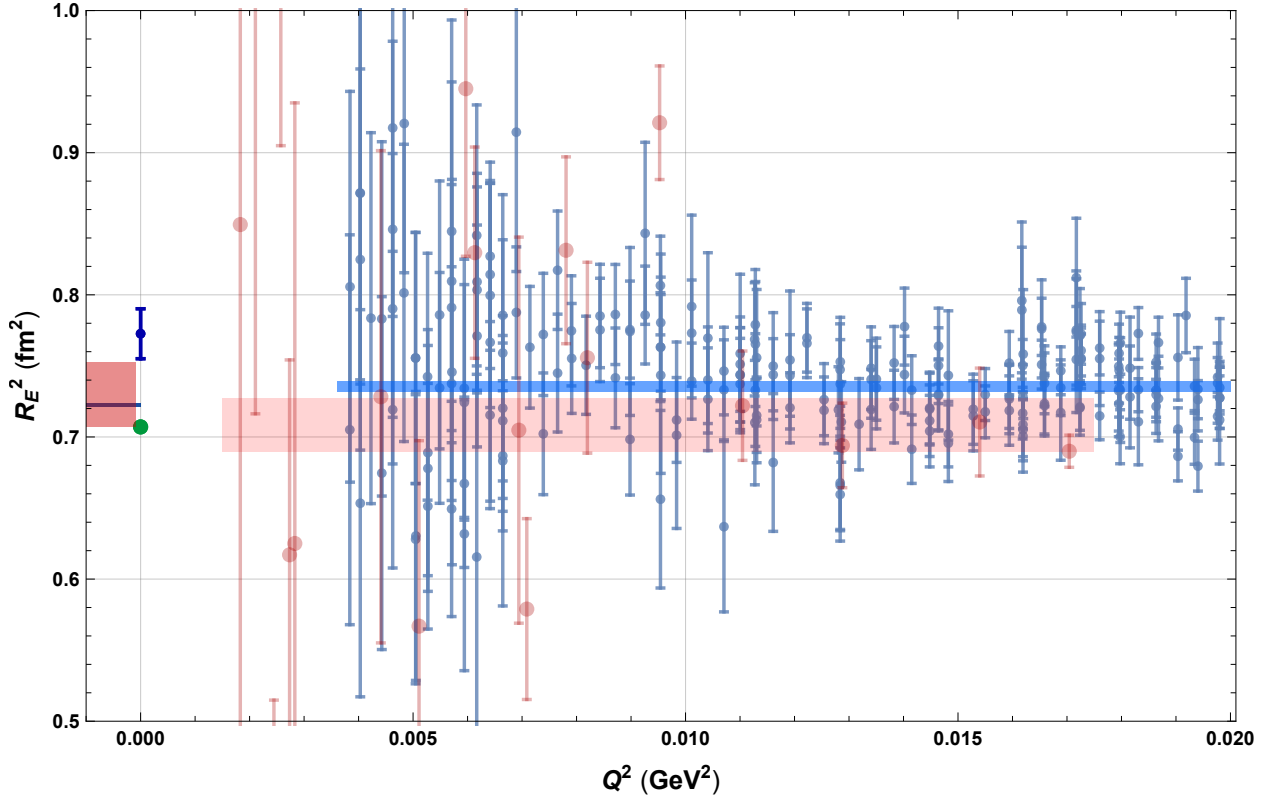


Figure 2: The quantity $R_E^2(Q^2)$ defined in Eq. (6) for the proton, whose value at 0 represents the proton charge-radius squared. The dark-blue and green points at 0 indicate the ep and μH values, respectively. The light-blue data points represent the dataset of Bernauer *et al.* [3, 4]. The light-red data points represent the ISR dataset of Mihovilović *et al.* [26]. The blue and red bands are the statistical averages of the corresponding datasets and are given numerically in the “Raw Average” column of Table 1. The bands below 0 show the results of a normalization-free determination (see Sec. 4.3 and “Normalization-free” column of Table 1) for comparison.

transverse density:²

$$\rho_{\perp}(b) = 2 \int_b^{\infty} dr \frac{r}{\sqrt{r^2 - b^2}} \rho_1(r) \quad (17a)$$

$$= \int_{-\infty}^{\infty} dz \rho_1(\sqrt{b^2 + z^2}). \quad (17b)$$

The two are thus related by the *Abel transform* [28, p. 351 et seq.]. It infers $\rho_{\perp} \geq 0$, for $\rho_1 \geq 0$, while the reverse is not necessarily true.

²Here we recall the following relations between the spherical and cylindrical Bessel functions:

$$J_0(x) = \frac{2}{\pi} \int_x^{\infty} dx' x' \frac{j_0(x')}{\sqrt{x'^2 - x^2}},$$

$$j_0(x) = \frac{1}{x} \int_0^x dx' x' \frac{J_0(x')}{\sqrt{x^2 - x'^2}},$$

as well as their orthogonality:

$$\int_0^{\infty} dQ Q J_l(Qb) J_l(Qb') = \frac{1}{b} \delta(b - b'),$$

$$\int_0^{\infty} dQ Q^2 j_l(Qr) j_l(Qr') = \frac{\pi}{2r^2} \delta(r - r').$$

4. Results from ep scattering data

4.1. Direct determination

We now proceed to obtaining the lower bound on the proton charge radius from ep scattering data. The first step is to convert the experimental data for $G_E(Q^2)$ to $R_E^2(Q^2)$, using the definition (6). The presently available data in the region well below the pion-pair production scale (here we chose $Q^2 < 0.02 \text{ GeV}^2$) are shown in Fig. 2. The light-blue points are from the dataset of Bernauer *et al.* [3, 4]. The light-red data points are from the recent initial-state radiation (ISR) experiment at MAMI [26], with the error bars indicating the statistical uncertainty only. The two points at $Q^2 = 0$ indicate the muonic-hydrogen (green) and Bernauer’s ep -scattering (dark-blue) values of the proton charge radius.

In principle, every data point in Fig. 2, at finite Q^2 , provides a lower bound on the proton charge radius. For a more accurate value, we can average over any subset of these data. In the figure, the horizontal blue band is the statistical average of Bernauer’s dataset, whereas the red band is the statistical average of the ISR dataset. The corresponding values for the lower bound are presented in the “Raw-average” column of Table 1.

This is how ideally the bound should be determined from

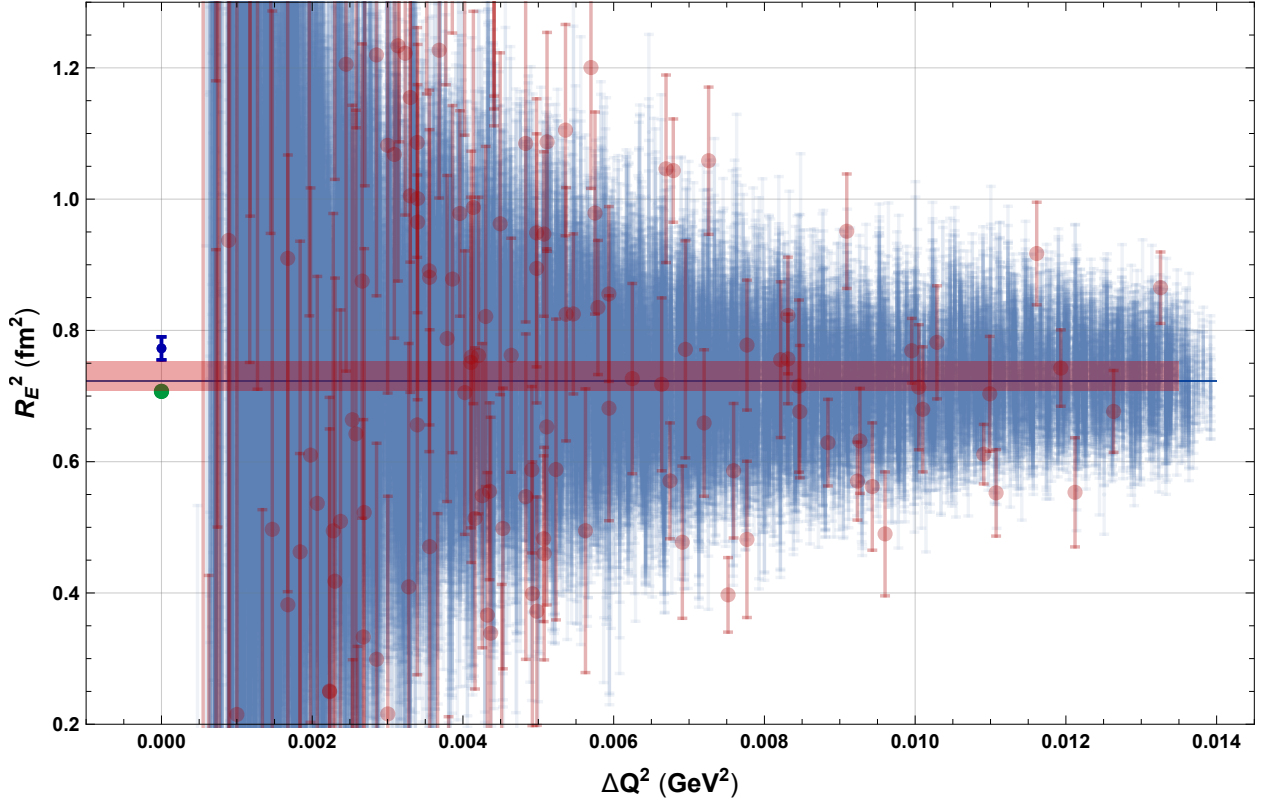


Figure 3: The quantity R_{ij}^2 , defined in Eq. (22) as a function of $\Delta Q^2 = Q_j^2 - Q_i^2$ for the proton, whose value at 0 represents the proton charge-radius squared. The dark-blue and green points at 0 indicate the ep and μH values, respectively. The light-blue data points represent the dataset of Bernauer *et al.* [3]. The light-red data points represent the ISR dataset of Mihovilović *et al.* [26]. The blue and red bands show the corresponding straight-line fits, which are interpreted as a normalization-free determination of the lower bound as reflected in the last column of Table 1.

the experimental data. However, the present experimental data have systematic uncertainties of which the most acute one is the unknown absolute normalization of the cross section. The Bernauer dataset, for example, is normalized in conjunction with the radius extraction. Thus, the data normalization and the extrapolation to $Q^2 = 0$ are done simultaneously in the same fit. Moreover, one can obtain an equally good representation of Bernauer’s data by using a lower value of the radius and different normalization factors [29]. In what follows, we attempt to deal with this problem and construct a lower bound which is independent of the overall normalization.

4.2. Overall normalization factor

To see how the normalization uncertainty affects the bound, let us suppose the experimental form factor has a small normalization error ϵ , such that $G_E^{(\text{exp})} = (1 + \epsilon) G_E$, with G_E having the usual interpretation. Then,

$$\begin{aligned} R_E^{2(\text{exp})}(Q^2) &= -\frac{6}{Q^2} \ln[(1 + \epsilon) G_E(Q^2)] \\ &= R_E^2(Q^2) - \frac{6}{Q^2} \ln(1 + \epsilon). \end{aligned} \quad (18)$$

If ϵ is positive, this is not a problem — the lower bound is preserved: $R_E^{2(\text{exp})}(Q^2) \leq R_E^2$, for $\epsilon \geq 0$. In the case of

$\epsilon < 0$, in a certain low- Q^2 region, the bound is violated:

$$R_E^{2(\text{exp})}(Q^2) \not\leq R_E^2, \quad \text{for } Q^2 < Q_0^2, \quad (19)$$

where Q_0 is the root of the following equation:

$$R_E^2(Q_0^2) - \frac{6}{Q_0^2} \ln(1 + \epsilon) = R_E^2. \quad (20)$$

Assuming Q_0 is small, we can use the expanded form of $R_E^2(Q^2)$ in Eq. (11), to find:

$$Q_0^2 = \sqrt{\frac{-6 \ln(1 + \epsilon)}{\frac{1}{20} \langle r^4 \rangle_E - \frac{1}{12} R_E^4}}. \quad (21)$$

For example, taking $\epsilon = -0.001$ and typical values of the radii [30], this equation gives $Q_0^2 \approx 0.01 \text{ GeV}^2$. Therefore, one strategy for avoiding the possible normalization issue is to drop the data below a certain Q^2 value from the lower-bound evaluation. A more efficient strategy is to use values at different Q^2 to cancel the overall normalization, as illustrated in what follows.

4.3. Towards a normalization-free bound

Having the form-factor data at a number of different points Q_i^2 (with $i = \overline{1, N}$), one may consider the following

quantity:

$$R_{ij}^2 \equiv \frac{-6}{Q_j^2 - Q_i^2} \ln \frac{G_E(Q_j^2)}{G_E(Q_i^2)} \quad (22)$$

It is a symmetric matrix with diagonal elements given by:

$$R_{ii}^2 = \frac{d}{dQ^2} \left[Q^2 R_E^2(Q^2) \right]_{Q^2=Q_i^2} = -6 \frac{G'_E(Q_i^2)}{G_E(Q_i^2)}. \quad (23)$$

In the region where the Taylor expansion of the proton form factor is rapidly convergent ($Q_i^2, Q_j^2 \ll 4m_\pi^2$), we have

$$R_{ij}^2 = R_E^2 - \left(\frac{1}{20} \langle r^4 \rangle_E - \frac{1}{12} R_E^4 \right) (Q_i^2 + Q_j^2) + \mathcal{O}(Q^4), \quad (24)$$

and therefore each of the elements provides a lower bound:

$$R_{ij}^2 \leq R_E^2, \quad \text{for any } i, j. \quad (25)$$

In Fig. 3, we plot the elements R_{ij} for the two datasets as a function of $\Delta Q^2 = Q_j^2 - Q_i^2$. The blue and red bands provide the two corresponding bounds obtained by using the `NONLINEARMODELFIT` routine of `MATHEMATICA` [31]. The latter values are given in the ‘‘Normalization-free’’ column of Table 1. In obtaining the bounds we have cut ΔQ^2 at both low and high ends.

Note that in removing the overall-normalization dependence, we assumed that all the data points of a given dataset have the same normalization factor. In reality, this is not the case, and a more refined analysis may be needed. For example, the experiment of Bernauer et al. has a complicated normalization procedure, involving 31 normalization factors (see Supplement in [4]), and one can manage to obtain significant shifts of the data points by a different fit of these factors [29]. These shifts could then be considered as a systematic normalization uncertainty which is only partially attributed to an overall normalization.

Nevertheless, one can identify subsets where the difference in normalization is overall and remove it using the R_{ij}^2 method described above. We have done that with two datasets of Higinbotham [29], generated from the data of Bernauer et al. [4], corresponding to significantly different radii. A subset of 106 data points in the very low- Q region ($Q^2 \leq 0.012 \text{ GeV}^2$) differs in an overall factor between the two datasets. Applying our method to this subset leads to: $R_E > 0.851(3)$ fm, for both datasets. We hence conclude that our method leads to a robust and accurate determination of the lower bound on R_E from the form-factor data even when they are prone to normalization uncertainties.

The lower bound resulting from the Bernauer dataset [$R_E > 0.850(1)$ fm] is very accurate and can be compared with the recent proton-radius extractions in Fig. 1. It is slightly above the μH values [5, 6], and the Garching measurement of the $2S - 4P$ transition frequency in H [9].

The low- Q^2 data are naturally preferred since, when we are in the region where the Taylor expansion of G_E is rapidly converging, the lowest Q^2 values of the function $R_E^2(Q^2)$ are the closest to the true value of the radius.

On the other hand, at lower Q^2 any imperfections in the experimental determination of the overall normalization of the form factor may lead to substantial corrections to the bound value.

Table 1: The lower-bound value of the proton charge radius, R_E (in fm), from two experimental data sets. The error corresponds to the 95% confidence interval (i.e., $\pm 2\sigma$). These results are represented by the bands in Figs. 2 and 3 with the corresponding color-coding.

Dataset	Raw Average	Normalization-free
Bernauer <i>et al.</i> [4]	0.857 \pm 0.003	0.850 \pm 0.001
Mihovilović <i>et al.</i> [26]	0.842 \pm 0.011	0.854 \pm 0.014

5. Conclusion

The electric form-factor data, obtained in the elastic electron-scattering experiments, provide a lower bound on the proton charge radius, rather than the charge radius itself; extraction of the latter requires in addition an extrapolation to zero momentum transfer. Our aim here is to leave the extrapolation issues out of the interpretation of ep data. We have established the function Eq. (6) sets a lower bound on the proton charge radius, Eq. (10), and attempted a first determination of this bound from the available data on $G_E(Q^2)$ at Q^2 below 0.002 GeV^2 . Our results for the two presently available datasets are given in Table 1. The last column therein shows the lower-bound values with reduced dependence on the overall normalization uncertainty.

The lower bound, $R_E > 0.850(1)$, resulting from the Bernauer dataset rules out the shaded area in Fig. 1. The figure also shows the results of recent proton-radius determinations. In particular, this ep bound is in disagreement with the muonic-hydrogen values (green dots). We emphasize that the present determination of the lower bound does not involve any fitting of the Q^2 -dependence with subsequent extrapolation to $Q^2 = 0$. Therefore, the discrepancy between the values extracted from muonic-hydrogen and ep scattering data is not due to the fitting or extrapolation of the latter.

With the forthcoming results of the PRad experiment [32, 33], we hope to obtain another precise determination of the lower bound on the proton charge radius. The PRad data will reach down to $2 \times 10^{-4} \text{ GeV}^2$ and include a simultaneous measurement of the Møller scattering. The latter will allow to drastically reduce the overall normalization uncertainty, which is the main problem of the present lower-bound determination.

Acknowledgements

We are grateful to Jan Bernauer, Michael Distler, Miha Mihovilović, Thomas Walcher for sharing their data with us and helpful communications; to Douglas Higinbotham for checking some of our results and an interesting discussion; to Patricia Bickert, Ashot Gasparian, Vadim Lensky, and Stefan Scherer for useful remarks on the manuscript. This work was supported by the Swiss National Science Foundation and the Deutsche Forschungsgemeinschaft (DFG) through the Collaborative Research Center 1044 [The Low-Energy Frontier of the Standard Model].

References

- [1] R. Hofstadter, R. W. McAllister, Electron scattering from the proton, *Phys. Rev.* 98 (1955) 217–218.
- [2] R. Hofstadter, Nuclear and nucleon scattering of high-energy electrons, *Ann. Rev. Nucl. Part. Sci.* 7 (1957) 231–316.
- [3] J. Bernauer, et al., High-Precision determination of the electric and magnetic form factors of the proton, *Phys. Rev. Lett.* 105 (2010) 242001.
- [4] J. C. Bernauer, M. O. Distler, J. Friedrich, T. Walcher, Electric and magnetic form factors of the proton, *Phys. Rev. C* 90 (2014) 015206.
- [5] R. Pohl, et al., The size of the proton, *Nature* 466 (2010) 213–216.
- [6] A. Antognini, et al., Proton structure from the measurement of 2S-2P transition frequencies of muonic hydrogen, *Science* 339 (2013) 417–420.
- [7] P. J. Mohr, B. N. Taylor, D. B. Newell, CODATA recommended values of the fundamental physical constants: 2010, *Rev. Mod. Phys.* 84 (2012) 1527–1605.
- [8] P. J. Mohr, D. B. Newell, B. N. Taylor, CODATA recommended values of the fundamental physical constants: 2014, *Rev. Mod. Phys.* 88 (2016) 035009.
- [9] A. Beyer, L. Maisenbacher, A. Matveev, R. Pohl, K. Khabarova, A. Grinin, T. Lamour, D. C. Yost, T. W. Hänsch, N. Kolachevsky, T. Udem, The rydberg constant and proton size from atomic hydrogen, *Science* 358 (2017) 79–85.
- [10] H. Fleurbaey, S. Galtier, S. Thomas, M. Bonnaud, L. Julien, F. Biraben, F. Nez, M. Abgrall, J. Guna, New Measurement of the 1S – 3S Transition Frequency of Hydrogen: Contribution to the Proton Charge Radius Puzzle, *Phys. Rev. Lett.* 120 (2018) 183001.
- [11] D. Borisyuk, Proton charge and magnetic rms radii from the elastic ep scattering data, *Nucl. Phys. A* 843 (2010) 59–67.
- [12] R. J. Hill, G. Paz, Model independent extraction of the proton charge radius from electron scattering, *Phys. Rev. D* 82 (2010) 113005.
- [13] X. Zhan, K. Allada, D. Armstrong, J. Arrington, et al., High Precision Measurement of the Proton Elastic Form Factor Ratio $\mu_p G_E/G_M$ at low Q^2 , *Phys. Lett. B* 705 (2011) 59–64.
- [14] I. Sick, Problems with proton radii, *Prog. Part. Nucl. Phys.* 67 (2012) 473–478.
- [15] K. Griffioen, C. Carlson, S. Maddox, Consistency of electron scattering data with a small proton radius, *Phys. Rev. C* 93 (2016) 065207.
- [16] G. Lee, J. R. Arrington, R. J. Hill, Extraction of the proton radius from electron-proton scattering data, *Phys. Rev. D* 92 (2015) 013013.
- [17] M. Horbatsch, E. A. Hessels, A. Pineda, Proton radius from electron-proton scattering and chiral perturbation theory, *Phys. Rev. C* 95 (2017) 035203.
- [18] C. Adamuscin, S. Dubnicka, A. Dubnickova, New value of the proton charge root mean square radius, *Prog. Part. Nucl. Phys.* 67 (2012) 479–485.
- [19] I. Lorenz, U. Meißner, H. Hammer, Y. Dong, Theoretical constraints and systematic effects in the determination of the proton form factors, *Phys. Rev. D* 91 (2015) 014023.
- [20] J. M. Alarcón, D. Higinbotham, C. Weiss, Z. Ye, Proton charge radius extraction from electron scattering data using dispersively improved chiral effective field theory, *hep-ph/1809.06373* (2018).
- [21] J. C. Bernauer, Avoiding common pitfalls and misconceptions in extractions of the proton radius, *nucl-th/1606.02159* (2016).
- [22] T. B. Hayward, K. A. Griffioen, Evaluation of low- Q^2 fits to ep and ed elastic scattering data, *nucl-ex/1804.09150* (2018).
- [23] X. Yan, D. W. Higinbotham, D. Dutta, H. Gao, A. Gasparian, M. A. Khandaker, N. Liyanage, E. Pasyuk, C. Peng, W. Xiong, Robust extraction of the proton charge radius from electron-proton scattering data, *Phys. Rev. C* 98 (2018) 025204.
- [24] C. F. Perdrisat, V. Punjabi, M. Vanderhaeghen, Nucleon Electromagnetic Form Factors, *Prog. Part. Nucl. Phys.* 59 (2007) 694–764.
- [25] M. Hoferichter, B. Kubis, J. Ruiz de Elvira, H. W. Hammer, U. G. Meiner, On the $\pi\pi$ continuum in the nucleon form factors and the proton radius puzzle, *Eur. Phys. J. A52* (2016) 331.
- [26] M. Mihovilović, et al., First measurement of proton’s charge form factor at very low Q^2 with initial state radiation, *Phys. Lett. B* 771 (2017) 194–198.
- [27] G. A. Miller, Transverse Charge Densities, *Ann. Rev. Nucl. Part. Sci.* 60 (2010) 1–25.
- [28] R. N. Bracewell, The Fourier transform and its applications, McGraw-Hill International Editions, 2000.
- [29] D. W. Higinbotham, private communication (2018).
- [30] M. O. Distler, J. C. Bernauer, T. Walcher, The RMS Charge Radius of the Proton and Zemach Moments, *Phys. Lett. B* 696 (2011) 343–347.
- [31] W. R. Inc., Mathematica, Version 11.3, 2018. Champaign, IL.
- [32] A. Gasparian for the PRad at JLab Collaboration, The PRad experiment and the proton radius puzzle, *EPJ Web Conf.* 73 (2014) 07006.
- [33] C. Peng, H. Gao, Proton Charge Radius (PRad) Experiment at Jefferson Lab, *EPJ Web Conf.* 113 (2016) 03007.